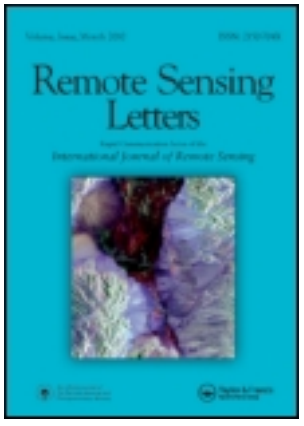

Remote Sensing Letters
Publication details, including instructions for authors and subscription information:
http://www.tandfonline.com/loi/trsl20

Empirical line calibration of WorldView-2 satellite imagery to reflectance data: using quadratic prediction equations

Grant William Staben [a b], Kirrilly Pfitzner [a], Renee Bartolo [a] & Arko Lucieer [b]

[a] Department of Sustainability, Environment, Water, Population & Communities, Environmental Research Institute of the Supervising Scientist, Darwin, NT, 0801, Australia

[b] School of Geography and Environmental Studies, University of Tasmania, Hobart, TAS, 7001, Australia

Available online: 23 Nov 2011

To cite this article: Grant William Staben, Kirrilly Pfitzner, Renee Bartolo & Arko Lucieer (2012): Empirical line calibration of WorldView-2 satellite imagery to reflectance data: using quadratic prediction equations, Remote Sensing Letters, 3:6, 521-530

To link to this article: http://dx.doi.org/10.1080/01431161.2011.609187

Remote Sensing Letters
Vol. 3, No. 6, November 2012, 521–530

Taylor & Francis
Taylor & Francis Group

Empirical line calibration of WorldView-2 satellite imagery to reflectance data: using quadratic prediction equations

GRANT WILLIAM STABEN*†‡, KIRRILLY PFITZNER†, RENEE BARTOLO† and ARKO LUCIEER‡

†Department of Sustainability, Environment, Water, Population & Communities, Environmental Research Institute of the Supervising Scientist, Darwin, NT 0801, Australia

‡School of Geography and Environmental Studies, University of Tasmania, Hobart, TAS 7001, Australia

(*Received 19 May 2011; in final form 27 July 2011*)

Obtaining accurate quantitative spectral information from raw multispectral satellite imagery requires the conversion of raw digital numbers (DNs) to units of radiance or reflectance. In this article, an empirical line method is used to calibrate WorldView-2 satellite imagery to surface reflectance. Prediction equations for the eight multispectral bands were developed using a non-linear relationship between sensor top-of-atmosphere spectral radiance (L_{TOA}) and surface reflectance values obtained from seven field targets. An accuracy assessment was undertaken by comparing image reflectance values against the surface reflectance values of 19 independent field targets. The overall accuracy based on the root mean square error (RMSE) for the eight bands ranged between 0.94% and 2.14% with the greatest variance in the near-infrared (NIR) bands. The results of this study show that empirical line methods can be used to successfully calibrate WorldView-2 satellite imagery to reflectance data.

1. Introduction

Before multispectral satellite imagery can be utilized for quantitative applications, a number of preprocessing steps, including geometric and radiometric corrections, need to be undertaken. A high degree of radiometric accuracy is required to standardize data for reliable or accurate change detection, and to relate remote sensing data to field-based measurements. To obtain quantitative information from multispectral satellite sensors such as WorldView-2, factors affecting the raw digital numbers (DNs) such as sensor characteristics, illumination geometry and atmospheric effects need to be removed (Smith and Milton 1999). Effects of the atmosphere, such as scattering and absorption, vary across the optical spectrum by either adding to or diminishing the surface radiance values recorded by the satellite sensor (Karpouzli and Malthus 2003, Hadjimitsis *et al*. 2009). A number of different methods have been developed to correct the effects of the atmosphere on satellite imagery. These include image-based

*Corresponding author. Email: gwstaben@postoffice.utas.edu.au

Remote Sensing Letters
ISSN 2150-704X print/ISSN 2150-7058 online
http://www.tandf.co.uk/journals
http://dx.doi.org/10.1080/01431161.2011.609187

methods (Chavez 1996), radiative transfer models (Vicente-Serrano *et al.* 2008) and empirical line method (Smith and Milton 1999, Karpouzli and Malthus 2003).

The empirical line method has been used to convert at-sensor radiance values to surface reflectance values for numerous multispectral satellites (Karpouzli and Malthus 2003, Hadjimitsis *et al.* 2009, Clark *et al.* 2010) and airborne hyperspectral sensors (Smith and Milton 1999). The technique is based on establishing a relationship between atmosphere sensor radiance (L_{TOA}) values and surface reflectance (P_S) values measured from calibration targets located within the image area. The P_S values of the calibration targets are measured using a field spectrometer and ideally should cover the range of albedo values found within the imagery. The L_{TOA} values are then extracted from the imagery and compared with the field-measured P_S values to define prediction equations that can be used to convert image-derived L_{TOA} to P_S values for each waveband (Smith and Milton 1999). According to Moran *et al.* (1990), the relationship between radiance and reflectance across the whole data range (0–100 %) is quadratic. However, correction of imagery using empirical line methods is typically based on a linear relationship, due to the design characteristics of the sensor used. It is also because the relationship between radiance and reflectance between 0% and 70 % has been found to be essentially linear, allowing interpolation with minimal error (Moran *et al*. 1990, Baugh and Groeneveld 2008, Clark *et al*. 2010). It must be noted that calibration of imagery using the empirical line method involves the simplification of a number of significant factors (Hadjimitsis *et al.* 2009). The assumptions are that both atmospheric conditions and illumination intensity are uniform across the image and that the image consists of features with Lambertian reflectance properties (Smith and Milton 1999). In addition, error may be introduced due to changes in atmospheric path length as a result of elevation differences between calibration targets and regions within the imagery (Baugh and Groeneveld 2008). The degree of deviation from these assumptions is an important factor affecting the accuracy of the prediction equations developed.

Karpouzli and Malthus (2003) used the empirical line methods to atmospherically correct IKONOS satellite images using nine calibration targets and reported highly satisfactory results. The authors highlighted the fact that the increased spatial resolution of the IKONOS sensor enabled a large number of targets to be identified, and suggested that increasing the number of calibration targets may contribute to the reduction of error between image- and field-measured P_S. The increased spatial resolution of the WorldView-2 sensor increases the potential number of homogeneous targets within an image. Two calibration panels and five field targets were used in this study as calibration targets to define non-linear equations for the eight WorldView-2 multispectral bands. A further 19 validation targets were then used to assess the reliability of the prediction equations derived for each spectral band. The aim of this study is to assess the ability of the empirical line method to convert very high spatial resolution multispectral WorldView-2 imagery from L_{TOA} to P_S values. As far as the authors are aware, this is the first published study that uses an empirical line method based on quadratic prediction equations to calibrate WorldView-2 imagery to surface reflectance data.

2. Methods

2.1 *Study area and data*

The study area is the Magela Creek catchment located in the Alligator Rivers Region (ARR), approximately 250 km east of Darwin, in the Northern Territory, Australia

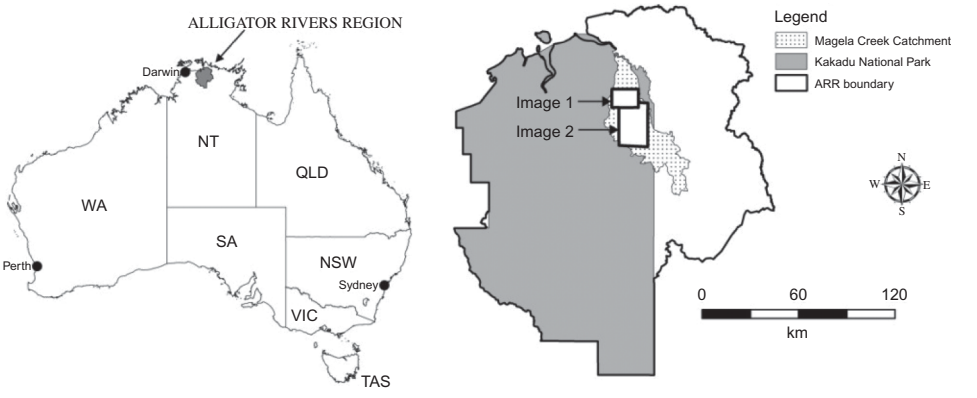

Figure 1. Location of the Alligator Rivers Region, study area (Magela Creek catchment) and the WorldView-2 image extent.

(figure 1). The ARR covers an area of ~28,000 km^2 and includes the world heritage listed Kakadu National Park. On 11 May 2010, two WorldView-2 multispectral images were acquired covering 620 km^2 of the Magela Creek catchment. As the requested study area exceeded the maximum swath width of the WorldView-2 satellite, two images were acquired during the overpass. The first image (Image 1) was captured at 11:14:28 Australian Central Standard Time (CST) with a mean off-nadir view angle of 18.3°, and the second image (Image 2) was captured approximately 13 seconds later at 11:14:41 CST with a mean off-nadir view angle of 16.8°. Images 1 and 2 covered an area of 183 and 479 km^2, respectively, with a 40 km^2 overlap between the two images. The WorldView-2 satellite collects data with an 11-bit dynamic range and consists of one panchromatic band (spatial resolution of 0.5 m) and eight multispectral bands (spatial resolution 2.0 m), for detailed sensor characteristics see Updike and Comp (2010).

2.2 *Image preprocessing*

Orthorectification of the imagery was undertaken using the sensor's rational polynomial coefficients (RPC) and ground control points (GCPs). The overall accuracy assessment of the orthorectification based on six independent GCPs resulted in an average root mean square error (RMSE) of 1.82 m. To account for sensor characteristics, the images were converted from DN to L_{TOA} spectral radiance values (Updike and Comp 2010) using equation (1):

$$L_{\mathrm{TOA}} = \frac{K_{\mathrm{Band}}\, Q_{\mathrm{Pixel,\,Band}}}{\Delta_{\lambda,\mathrm{Band}}}, \tag{1}$$

where L_{TOA} represents TOA spectral radiance image pixels in a given band (Wm^{-2} sr^{-1} μm^{-1}); K_{Band} is the absolute radiometric calibration factor (Wm^{-2} sr^{-1} count^{-1}) for a given band; $Q_{\mathrm{Pixel,Band}}$ represents the radiometrically corrected image pixels (DN); and $\Delta_{\lambda,\mathrm{Band}}$ is the effective bandwidth (μm) for a given band at wavelength, λ. The absolute calibration (K_{Band}) and effective bandwidth ($\Delta_{\lambda,\mathrm{Band}}$) parameters for each band are obtained from the metadata supplied with the imagery.

2.3 *Field spectra*

This study utilized a combination of both calibration panels and field targets to convert L_{TOA} values to P_S. Smith and Milton (1999) suggested that field targets used for empirical line correction should have the following characteristics: be spectrally homogeneous; be near Lambertian and horizontal; be devoid of vegetation; cover an area several times the pixel size of the sensor; and cover a range of reflectance values. In this study a total of 24 targets were measured in the field along with two calibration panels. The two calibration panels and five selected field targets (table 1) were used to derive the prediction equation between L_{TOA} and P_S for each waveband, while the remaining 19 targets (table 2) were used to assess the accuracy of the prediction equations.

Ideally, field reflectance spectra used to calibrate imagery should be collected at the time of image capture (Baugh and Groeneveld 2008). However, due to numerous scheduled image capture dates proposed by DigitalGlobe (Longmont, CO, USA) combined with unseasonal adverse weather conditions, field spectra were collected on 5 days over a 3-week period during May 2010 (collection dates; 6, 7, 11, 13 and 27 May). Field spectra were collected between the hours of 10:00 and 15:00 local time using a FieldSpecPro-FR spectrometer (Analytical Spectral Devices (ASD) Inc., Boulder, CO, USA) (covering 350–2500 nm) with a 25° field of view (FoV) at nadir. Spectra were captured using a boom extension on a tripod at a height of 1 m for terrestrial targets and 0.5 m for targets over water, resulting in a ground view of ~44 cm for terrestrial targets and ~22 cm over water. A Labsphere Spectralon® (Labsphere Inc., North Sutton, NH, USA) white reference panel was used to obtain reflectance data with the number of white reference readings acquired for each target dependent on the stability of the atmospheric conditions. A minimum of one and a maximum of four spectral samples were collected between each white reference and dark current calibration, and the averaging sample spectrum was set to 25. The number of samples obtained for each target was dependent on the variance observed within the target, with between 9 and 25 samples collected per target. The area subsampled for most targets was 25 m^2. However, larger areas were sampled for targets such as synthetic bowling-green, golf green, rock outcrop and bitumen road, as these targets could be easily identified within the imagery. The location of each target was recorded using a handheld GPS with an accuracy of ±3 m. The majority of targets, with the exception of the open water targets from Jabiluka Billabong, were located within

Table 1. Description and mean coefficient of variation for targets used in the calibration of the WorldView-2 imagery.

Target ID	Target description	CoV
C1[c]	(~95%) Tyvec® calibration panel	0.97
C2[c]	(~67%) White calibration panel	2.77
C3[c]	Sports field grass	6.96
C4[d]	Synthetic bowling green	15.58
C5[d]	Asphalt road	17.13
C6[e]	Open water Jabiluka Billabong	9.29
C7[e]	Open water Jabiluka Billabong	9.31

Notes: CoV is the mean coefficient of variation of each target based on ASD field spectra wavelength of 400–1040 nm.
Spectra collection date: [c] = 11 May 2010, [d] = 13 May 2010, [e] = 27 May 2010.

Table 2. Description and mean coefficient of variation for targets used in validation of the calibrated WorldView-2 imagery.

Target ID	Target description	CoV
V1[a]	Sports field grass	13.23
V2[a]	Open water Jabiru Town Lake	14.10
V3[a]	Open water Jabiru Town Lake	55.82
V4[b]	Asphalt road	5.52
V5[b]	Sports field grass	9.42
V6[c]	Sports field grass	4.31
V7[c]	Sports field grass	5.91
V8[c]	Sports field grass	7.88
V9[c]	Sports field grass	12.25
V10[c]	Golf green	8.86
V11[d]	Builders sand	6.89
V12[d]	Sand/blue stone	31.86
V13[d]	Sand/concrete slab	9.83
V14[d]	Native grass	17.43
V15[d]	Rock outcrop	39.28
V16[d]	Bare earth (scrape)	13.59
V17[e]	Open water Jabiluka Billabong	10.18
V18[e]	Bare earth	13.76
V19[e]	White road base	14.64

Notes: CoV is the mean coefficient of variation of each target based on ASD field spectra wavelength 400–1040 nm.
Spectra collection date: [a] = 6 May 2010, [b] = 7 May 2010, [c] = 11 May 2010, [d] = 13 May 2010, [e] = 27 May 2010.

Image 2. The only target located within the overlap of the two images was the rock outcrop (V15 in table 2). Two calibration panels were used in this project, a double layer of Tyvec® (DuPont, Wilmington, DE, USA) covering an area of 5.9 × 5.9 m and a 4.8 × 4.8 m heavy duty white polyester tarpaulin. These materials were selected as they represented targets with high reflectance values (∼95% and ∼67%) and previous laboratory spectral measurements had also identified the suitability of these targets for use as calibration panels (Pfitzner *et al*. 2010).

The panels were laid out on the Jabiru sports field, on the morning of the satellite overpass, and spectra were collected immediately after the satellite overpass. Targets used for the prediction equation were selected based on the fact that they represented a range of reflectance values (dark to bright values), were spectrally homogeneous (summarized by mean coefficient of variation (CoV)) and were likely to be invariant features. The one vegetation target used for the prediction equation was measured ∼30 minutes after the image capture.

2.4 *Empirical line calibration*

The averaged field spectra (P_S) were resampled to the relative spectral response of each WorldView-2 waveband. The average L_{TOA} values corresponding with each calibration panel and field target were then extracted from the imagery. The number of L_{TOA} pixels extracted for each target ranged between 2 (C2) and 95 (V15) pixels with the majority characterized by 6 pixels. Where the extent of a target could be identified in the image, pixels were selected to avoid mixed pixels and reduce adjacency effects. A non-linear quadratic relationship equation (2) was fitted between L_{TOA} and P_S:

$$y = a + b_1 x + b_2 x^2, \tag{2}$$

where y is the response representing P_S; x is the predictor representing L_{TOA}; a is the intercept; and b_1 and b_2 are the fitting coefficients. The intercept (a) represents the additive effect due to atmospheric path radiance and the slope parameters (b_1, b_2) represent the correction for atmospheric attenuation (Karpouzli and Malthus 2003, Hadjimitsis *et al.* 2009).

2.5 *Accuracy assessment*

The overall accuracy of the empirical line calibration was assessed by comparing image-derived P_S values with field-measured P_S for the 19 validation targets. Summary statistics were obtained to assess the performance of each spectral band and each individual validation target, using the RMSE equation (3), and the mean absolute percent error (MAPE) equation (4), which enables the assessment of the relative error for each target. The RMSE and MAPE are computed as follows:

$$\text{RMSE} = \frac{\sqrt{\sum_{i=1}^{n} (p_i - r_i)^2}}{n}, \tag{3}$$

$$\text{MAPE} = \frac{1}{n} \sum_{i=1}^{n} \left| \left(\frac{p_i - r_i}{r_i} \right) 100 \right|, \tag{4}$$

where p_i represents the predicted reflectance value for band i; r_i represents the field-measured reflectance; and n represents the number of bands (eight) for the assessment of individual targets or (19) for the assessment of each spectral band. As the validation target V15 (rock outcrop) occurred in the overlap regions of the images, it was used to evaluate the effect that the different off-nadir view angles (18.3° Image 1 and 16.8° Image 2) had on the predicted P_S values derived from each image.

3. Results and discussion

3.1 *Prediction equations*

The combination of calibration panels and field targets enabled the development of a non-linear relationship between L_{TOA} and P_S. A total of seven targets were used to derive the prediction equation, resulting in statistically significant relationships for each waveband (coefficient of determination $R^2 = 0.99$, $p < 0.0001$, 99% confidence level). The quadratic relationship between L_{TOA} and P_S for the targets used in this study is illustrated in figure 2. The use of the bright reflectance calibration panels ensured that predicted P_S values were interpolated within the bounds of the prediction equations. The distribution of calibration targets across each of the wavebands shows that the highest reflectance values were represented by Tyvec® and the white calibration panels with average P_S of ~95% to ~67%, respectively, while the range of reflectance values represented by other calibration targets was lower (e.g. 0.08–38% in the NIR-2 band). Importantly, the 11-bit dynamic range of the WorldView-2 sensor

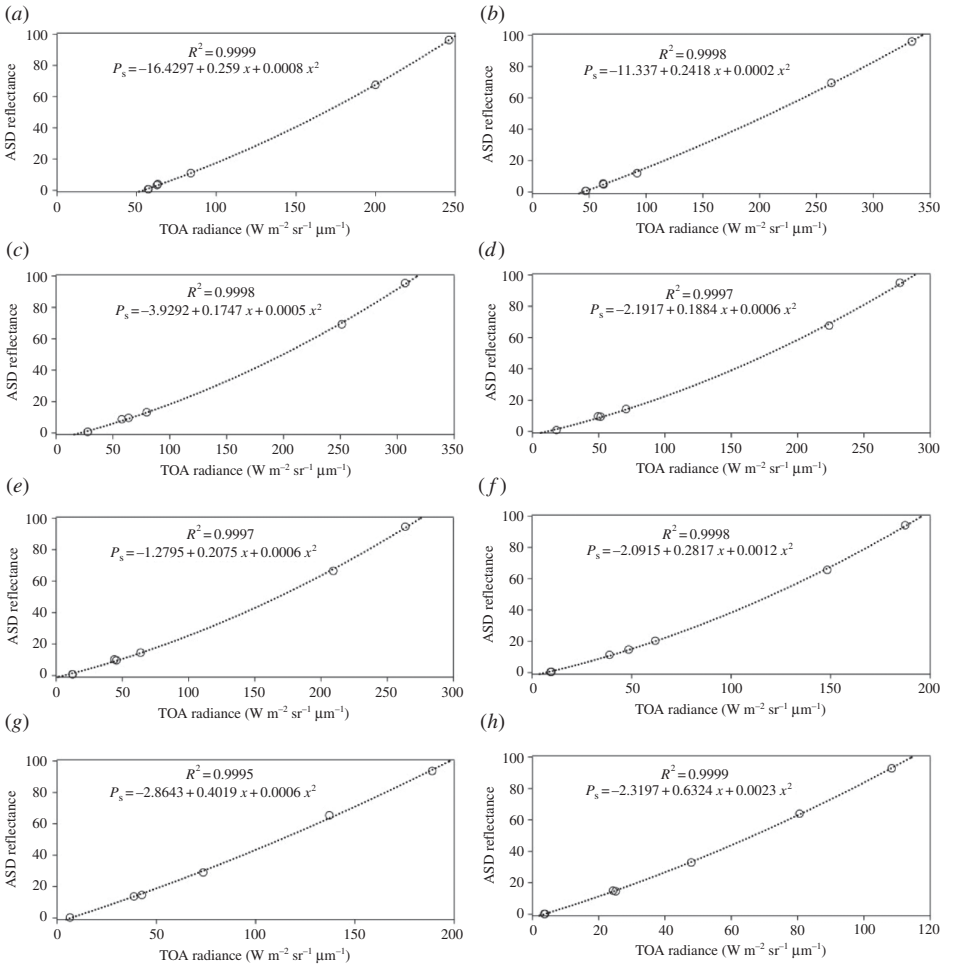

Figure 2. Non-linear regression lines and prediction equations developed for each WorldView-2 waveband: (*a*) Band 1, (*b*) Band 2, (*c*) Band 3, (*d*) Band 4, (*e*) Band 5, (*f*) Band 6, (*g*) Band 7 and (*h*) Band 8.

did not saturate at the high reflectance levels for the two calibration panels used in this project. Correction for atmospheric path radiance (represented by the intercept of the *x*-axis) was greatest in Band 1 (coastal), Band 2 (blue) and Band 3 (green), while the remaining five bands recorded similar values with the lowest value recorded for Band 5 (red) (figure 2).

3.2 *Validation targets*

Summary statistics for each band are presented in table 3. The overall RMSE values for each band show that there was a high degree of agreement between the satellite-derived P_S values and the field-measured P_S values for the 19 validation targets. Five of the eight bands recorded RMSE values below 1.5% with the coastal band recording the lowest value 0.94%. The red-edge and the two NIR bands recorded the highest

Table 3. Summary statistics derived from the validation targets for each waveband.

Band	RMSE (%)	MAPE (%)
Coastal (1)	0.94	18.39
Blue (2)	1.05	14.01
Green (3)	1.20	11.48
Yellow (4)	1.29	13.75
Red (5)	1.36	16.78
Red edge (6)	1.86	16.02
NIR-1 (7)	2.13	25.97
NIR-2 (8)	2.14	44.83

Notes: RMSE, root mean square error; MAPE, mean absolute percent error; NIR, near-infrared. RMSE evaluates the overall accuracy, while MAPE assesses the relative error for each band.

Table 4. Summary statistics for each validation target.

Target ID	Target description	RMSE (%)	MAPE (%)
V1[a]	Sports field grass	1.32	4.71
V2[a]	Open water Jabiru Town Lake	0.45	51.44
V3[a]	Open water Jabiru Town Lake	0.53	134.37
V4[b]	Asphalt road	0.74	7.35
V5[b]	Sports field grass	2.08	8.97
V6[c]	Sports field grass	0.88	8.93
V7[c]	Sports field grass	1.25	13.92
V8[c]	Sports field grass	0.87	4.14
V9[c]	Sports field grass	0.69	6.73
V10[c]	Golf green	2.12	20.52
V11[d]	Builders sand	1.17	4.72
V12[d]	Sand/blue stone	4.63	21.16
V13[d]	Sand/concrete slab	1.80	5.88
V14[d]	Native grass	0.54	2.54
V15[d]	Rock outcrop (Image 1)[†]	0.86	3.45
V15[d]	Rock outcrop (Image 2)[†]	1.25	4.18
V16[d]	Bare earth (scrape)	0.81	6.35
V17[e]	Open water Jabiluka Billabong	0.37	70.01
V18[e]	Bare earth	1.28	5.19
V19[e]	White road base	0.93	1.86

Notes: RMSE, root mean square error; MAPE, mean absolute percent error. RMSE evaluates the overall accuracy, while MAPE assesses the relative error for each target. Spectra collection date: [a] = 6 May 2010, [b] = 7 May 2010, [c] = 11 May 2010, [d] = 13 May 2010, [e] = 27 May 2010.
[†]Image statistics were derived from Image 1 and Image 2.

RMSE values. However, the MAPE values (which assess relative error) show that the red-edge band recorded errors similar to the bands in the visible portion of the electromagnetic spectrum.

The overall RMSE value based on the mean of the eight bands for the 19 validation targets was low with values ranging from 0.37 to 4.63 (table 4). While the RMSE values were generally low across the range of targets, the MAPE values clearly show

that there were significant errors in the three open water targets (V2, V3 and V17). The relative error in the open water targets is largely distributed across the eight wavebands; however, the highest MAPE values were recorded in the two NIR bands. The increased error in the NIR bands for the three open water targets is also evident in the summary statistic for each waveband (table 3).

A number of factors may have contributed to the comparatively large RMSE values observed for target V12 (sand/blue stone). The target is a mixture of two endmembers of sand, and a stone aggregate used to make concrete and insufficient field spectral samples may have been collected to characterize this heterogeneous target. Also the area is potentially variable over time with new deposits of sand or stone. There may have also been positional error between the actual L_{TOA} values extracted from imagery and the field-based P_S. There was a high degree of accuracy with the eight vegetation targets which had RMSE values ranging from 0.54% to 2.12% and MAPE values ranging from 2.54% to 20.52%. The highest error was recorded by the golf green (V10); this error may be due to the changes in moisture content due to watering, and as a result of the 3-hour time difference between the image overpass and field spectra captured for this target. The validation targets with the highest reflectance values across all wavebands were V11 builder's sand (P_S values between 0.11% and 38%) and V19 white road base (P_S values between 29% and 43%), the most homogeneous and invariant targets measured. The predicted P_S values for targets V11 and V19 further emphasized the quadratic relationship between L_{TOA} and P_S. Both targets recorded low RMSE and MAPE values with the observed L_{TOA} and P_S values for each waveband falling close to or on the prediction line. The close agreement between the predicted and the observed values for targets V4, V13, V16 and V18 and the difference in the field spectra and image acquisition dates highlight the invariant nature of these targets.

The WorldView-2 spectral signatures predicted for V15 (rock outcrop) from the two different off-nadir view angles and the ASD field-measured P_S are presented in figure 3. The spectral signatures and the RMSE and MAPE values for each image demonstrate that the prediction equations were able to account for the different view angles with very little variance in the predicted P_S values for each image.

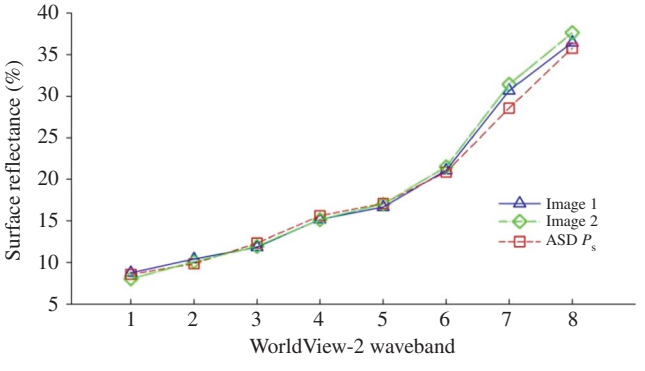

Figure 3. Comparison of the WorldView-2 spectral signature for the validation target (rock outcrop): Image 1 and Image 2 are the predicted P_S values derived from different view angles and the ASD P_S is the field-measured P_S.

4. Conclusion

The combination of both calibration panels and image targets enabled the development of prediction equations covering the full range of albedo values within the image. The high accuracy achieved in the geometric correction of the imagery and the spatial and radiometric resolution of the WorldView-2 sensor enabled calibration targets to be easily identified in the imagery. Importantly, the calibration targets used ensured that the predicted P_S values were interpolated within the bounds of the prediction equations. The results of this study show that the empirical line method using quadratic prediction equations can be used to successfully calibrate the eight multispectral bands of the WorldView-2 satellite image to surface reflectance.

Acknowledgements

The authors acknowledge Sally-Anne Atkins, Annamarie Beraldo and John Lowry for help with collection of field data, and people and organizations for access to their land/property, traditional owners of Kakadu National Park, Jabiru Sports Club, Jabiru Golf Club, Jabiru Council and Hansons Heidelberg Cement Group.

References

Baugh, W.M. and Groeneveld, D.P., 2008, Empirical proof of the empirical line. *International Journal of Remote Sensing*, **29**, pp. 665–672.

Chavez Jr., P.S., 1996, Image based atmospheric corrections – revisited and improved. *Photogrammetric Engineering and Remote Sensing*, **62**, pp. 1025–1036.

Clark, B., Suomalainen, J. and Pellikka, P., 2010, A comparison of methods for the retrieval of surface reflectance factor from multi-temporal SPOT HRV, HRVIR and HRG multispectral satellite imagery. *Canadian Journal of Remote Sensing*, **36**, pp. 397–411.

Hadjimitsis, D., Clayton, C. and Retalis, A., 2009, The use of selected pseudo-invariant targets for the application of atmospheric correction in multi-temporal studies using satellite remotely sensed imagery. *International Journal of Applied Earth Observation and Geoinformation*, **11**, pp. 192–200.

Karpouzli, E. and Malthus, T., 2003, The empirical line method for the atmospheric correction of IKONOS imagery. *International Journal of Remote Sensing*, **24**, pp. 1143–1150.

Moran, M.S., Jackson, R.D., Hart, G.F., Slater, P.N., Bartell, R.J., Biggar, S.F., Gellman, D.I. and Santer, R.P., 1990, Obtaining surface reflectance factors from atmospheric and view angle corrected SPOT1 HRV data. *Remote Sensing of Environment*, **32**, pp. 203–214.

Pfitzner, K., Staben, G. and Bartolo, R., 2010, The spectral reflectance of common artificial pseudo invariant materials. *Proceedings of the 15th Australasian Remote Sensing & Photogrammetry Conference (ARSPC)*, 13–17 September 2010, Alice Springs, Australia.

Smith, G.M. and Milton, E.J., 1999, The use of the empirical line method to calibrate remotely sensed data. *International Journal of Remote Sensing*, **20**, pp. 2635–2662.

Updike, T. and Comp, C., 2010, *Radiometric use of WorldView-2 Imagery*, Technical Note (Longmont, CO: DigitalGlobe).

Vicente-Serrano, S.M., Pérez-Cabello, F. and Lasanta, T., 2008, Assessment of radiometric correction techniques in analyzing vegetation variability and change using time series of Landsat images. *Remote Sensing of Environment*, **112**, pp. 3916–3934.